Chemical Engineering Journal 150 (2009) 455–461

Contents lists available at ScienceDirect

Chemical Engineering Journal

journal homepage: www.elsevier.com/locate/cej

Adsorption of phenol by oil–palm-shell activated carbons in a fixed bed

Aik Chong Lua*, Qipeng Jia

School of Mechanical and Aerospace Engineering, Nanyang Technological University, 50 Nanyang Avenue, Singapore 639798, Republic of Singapore

ARTICLE INFO

Article history:
Received 26 September 2007
Received in revised form 15 January 2009
Accepted 20 January 2009

Keywords:
Activated carbon
Oil–palm shell
Kinetic modelling
Fixed bed reactor
Adsorption

ABSTRACT

Steam-activated carbons from oil–palm shells were prepared and used in the adsorption of phenol. The activated carbon had a well-developed non-micropore structure which accounted for 55% of the total pore volume. The largest Brunauer–Emmett–Teller (BET) surface area of the activated carbon was 1183 m^2/g with a total pore volume of 0.69 cm^3/g using N_2 adsorption at 77 K. Experimental tests on the adsorption of phenol by the activated carbons were carried out in a fixed bed. The aqueous phase adsorption isotherms could be described by the Langmuir equation. The effects of the operation conditions of the fixed bed on the breakthrough curve were investigated. A linear driving force model based on particle phase concentration difference (LDFQ model) was used to simulate the fixed bed adsorption system. The model simulations agreed with the experimental data reasonably well.

1. Introduction

Phenolic compounds and their derivatives are classified as priority pollutants. They enter into environment through industries such as coal conversion, petroleum refining, textile and pharmaceutical, as well as large-scale use of herbicides, insecticides and pesticides in agriculture [1]. Phenols are also released as intermediate products during microbial degradation of pesticides or some other xenobiotics [2]. Various methods are available to remove phenol. Adsorption of phenol by activated carbons is a very effective and most frequently used method. In liquid phase adsorption applications, a fixed bed column is the typical operation unit which is also true for phenol adsorption.

The adsorption performance of *p*-nitrophenol onto granular activated carbons in 25 °C aqueous solution for a dynamic process was investigated by Chern and Chien [3]. A series of column tests were performed to determine the breakthrough curves with varying bed depths and water flow rates. They applied the constant pattern wave approach using the Freundlich isotherm model to fit the experimental breakthrough curves. Pan et al. [4] combined the constant pattern wave approach theory and adsorption isotherm to determine the breakthrough curves of a fixed bed adsorption system for two adsorbate solutions. They carried out dynamic experiments at different conditions for phenol, *p*-nitrophenol and macro-reticular polymeric resin adsorbent systems. The breakthrough curves predicted by the model and those of the experimental runs were in satisfactory agreement. In their study, a correlation was proposed to predict the volumetric mass transfer coefficient in the liquid phase.

Activated carbon adsorption may have an edge over other methods in terms of cost especially if the starting materials for the activated carbons are biomass waste products. Oil–palm shell is one of the by-products of the palm oil industry. Malaysia, which is the world's largest palm oil producing country, generates about 4.3 million tonnes of fruit shells and 8.6 million tonnes of fibres every year [5]. Conversion of these wastes into activated carbons would add value to this biomass and, in addition, the conversion from wastes may be able to reduce the price of commercial activated carbons. Oil–palm shell is used as a suitable precursor for preparing activated carbon because of its hardness, high carbon content and low ash content [6].

In this study, the oil–palm-shell activated carbons were used to adsorb phenol using a fixed bed adsorption system. This type of activated carbon has shown to be a good adsorbent for phenol solution [7]. The effects of the feed volume flow rate, the initial phenol concentration in the feed and the height of the fixed bed on the effective load of the fixed bed were studied. Further, modelling on the adsorption dynamics of the fixed bed was presented and finally the correlation between the model and the experimental data was compared.

2. Theory

2.1. Adsorption equilibrium

Adsorption isotherms are used to relate the mechanics in which the adsorbates will interact with the adsorbents. Equilibrium adsorption results by the authors [8] have indicated that the

* Corresponding author. Tel.: +65 67905535; fax: +65 67924062.
E-mail address: maclua@ntu.edu.sg (A.C. Lua).

1385-8947/$ – see front matter © 2009 Elsevier B.V. All rights reserved.
doi:10.1016/j.cej.2009.01.034

Nomenclature

b_L	Langmuir adsorption equilibrium constant
c	aqueous phase concentration (mg cm^{-3})
c_0	Initial aqueous solution concentration (mg cm^{-3})
c_e	equilibrium aqueous phase concentration (mg cm^{-3})
c_s	aqueous phase concentration at particle surface (mg cm^{-3})
d_p	particle diameter (cm)
D_p	pore diffusion coefficient (cm^2 s^{-1})
D_s	surface diffusion coefficient (cm^2 s^{-1})
H	bed column height (cm)
k_f	fluid-to-particle mass transfer coefficient (s^{-1})
k_s	particle phase mass transfer coefficient (g cm^{-3} s^{-1})
K_S	overall mass transfer coefficient (g cm^{-3} s^{-1})
Pe	Peclet number
q	solid phase average concentration (mg g^{-1})
q_0	solid phase concentration in equilibrium with c_0 (mg g^{-1})
q_e	equilibrium solid phase concentration (mg g^{-1})
q_m	solid phase maximum concentration corresponding to monolayer saturation coverage (mg g^{-1})
q_s	solid phase concentration at particle surface (mg g^{-1})
r	particle radius (cm)
R	equilibrium parameter for adsorption
$\mathrm{Re_p}$	particle Reynolds number ($\mathrm{Re_p} = u\varepsilon_b d_p \rho_f/\mu$)
t	time (s)
t_0	characteristic time constant
u	interstitial velocity of the fluid in the fixed bed (cm s^{-1})
u_c	velocity of the concentration wave front (cm s^{-1})
x	non-dimensional effluent concentration ($x = c/c_0$)
x_e	non-dimensional effluent concentration at equilibrium ($x_e = c_e/c_0$)
x_s	non-dimensional aqueous concentration at particle surface ($x_s = c_s/c_0$)
y	dimensionless solid phase concentration ($y = q/q_0$)
y_e	dimensionless solid phase concentration at equilibrium ($y_e = q_e/q_0$)
y_s	non-dimensional solid phase concentration at particle surface ($y_s = q_s/q_0$)
z	axial distance (cm)

Greek symbols

ε_b	void fraction of the bed (ε_b is the ratio of the void volume to the total volume of the bed)
ϕ_s	correlation parameter
μ	fluid dynamic viscosity (dyn s cm^{-2})
θ	dimensionless parameter ($\theta = K_s\tau/\rho_b$)
ρ_b	bulk density of bed (g cm^{-3})
ρ_f	fluid density (g cm^{-3})
τ	adjusted time (s)
ζ	correlation parameter

Langmuir isotherm equation can best describe the adsorption isotherms of phenol onto activated carbons. Hence, the Langmuir isotherm equation would be used to depict the adsorption isotherms of the activated carbons. The Langmuir isotherm equation is

$$q_e = q_m \frac{b_L c_e}{1 + b_L c_e} \tag{1}$$

where c_e and q_e are the concentrations in the aqueous and solid phases, respectively, at equilibrium, and q_m is the maximum concentration in the solid phase that corresponds to monolayer saturation coverage. The constant b_L is the adsorption equilibrium constant which is the ratio of adsorption to desorption rates. Non-linear least-squares analysis was used to obtain the parameters in the isotherms.

2.2. Dynamic model description

Comparative studies between the dynamic models of liquid phase adsorption by activated carbons and experimental results for fixed beds have been reported in the literature such as Chern and Chien [3], Sotelo et al. [9] and Pan et al. [4]. Simulations are used to determine the time duration and mechanics of the occurrence of breakthroughs. The relevant breakthrough curves provide information for designing a specified fixed bed adsorption system. For non-linear isotherm systems, explicit equations for the breakthrough curves of fixed bed adsorption processes with adsorption isotherms are developed by the constant pattern wave approach using a constant driving force model in the liquid phase. For a quick estimation of the breakthrough behaviour of an adsorption column, simplified treatments can be utilized with reasonable assumptions. With these assumptions, analytical solutions can be obtained.

The speed of mass transfer zone movement along the fixed bed can be derived by the mass balance equation of the bed. For favourable isotherm relation such as that of the Langmuir type, concentration profiles moving along the column can be described as constant patterns. Constant pattern front (CPF) was first described by Bohart and Adams [10] for irreversible adsorption. CPF is derived on the assumption that the fluid moves as a plug flow through the bed at a constant actual (interstitial) velocity u, instantaneous equilibrium of the solute in the bulk fluid with the adsorbate, no axial dispersion and isothermal conditions. The fixed bed modelling equations can be simplified to a mass balance on the solute

$$\frac{\partial c}{\partial t} + u\frac{\partial c}{\partial z} + \frac{\rho_b}{\varepsilon_b}\frac{\partial q}{\partial t} = 0 \tag{2}$$

where c is the aqueous phase concentration, t is the time, z is the axial distance from the bed inlet, ε_b is the void fraction of the bed, ρ_b is the bulk density of the bed and q is the adsorbate loading/unit mass of adsorbent particles. The relationship between q and c can be expressed by an appropriate adsorption isotherm. In the mass conservation equation, c is a function of z and t, i.e., $c = f(z, t)$. Therefore, the velocity u_c of the concentration wave front which is $\partial z/\partial t$ at constant c, can be expressed by the rules of implicit partial differentiation and is given by

$$u_c = \left(\frac{\partial z}{\partial t}\right)_c = -\frac{(\partial c/\partial t)}{(\partial c/\partial z)} \tag{3}$$

The superficial fluid velocity is $\varepsilon_b u$. Combining Eqs. (2) and (3), the velocity of the concentration wave front can be expressed as

$$u_c = \frac{u}{1 + (\rho_b/\varepsilon_b)dq/dc} \tag{4}$$

Eq. (4) gives the velocity of the concentration wave front for the solute in terms of the interstitial fluid velocity and the slope, dq/dc, of the adsorption isotherm.

Eq. (4) indicates the velocity of the concentration wave front that moves through the bed. If the adsorption isotherm is curved, for a favourable isotherm of the Freundlich or Langmuir type, the wave front steeps with time until a CPF is developed. When the constant pattern profile is established, the speed of movement of the point on the mass transfer zone is constant regardless of concentration. With the constant pattern wave moving at a constant value, the

aqueous phase concentration can be expressed as a function of an adjusted time. This adjusted time, τ, is defined as

$$\tau = t - \frac{z}{u_c} \tag{5}$$

Substituting Eq. (5) into Eq. (2) on the basis of substituting $c(t, z)$ with $c(\tau)$ gives

$$\left(1 - \frac{u}{u_c}\right)\frac{dc}{d\tau} + \frac{\rho_b}{\varepsilon_b}\frac{dq}{d\tau} = 0 \tag{6}$$

Integrating Eq. (6) gives

$$\int_0^c \left(1 - \frac{u}{u_c}\right) dc + \int_0^q \frac{\rho_b}{\varepsilon_b} dq = 0 \tag{7}$$

and

$$\left(1 - \frac{u}{u_c}\right) c + \frac{\rho_b}{\varepsilon_b} q = 0 \tag{8}$$

Applying the initial boundary conditions, $c = c_0$ and $q = q_0$, Eq. (8) becomes

$$\left(1 - \frac{u}{u_c}\right) c_0 + \frac{\rho_b}{\varepsilon_b} q_0 = 0 \tag{9}$$

Comparing Eqs. (8) and (9), the following relationship is applicable as a condition of the constant pattern:

$$\frac{q}{q_0} = \frac{c}{c_0} \tag{10}$$

where c_0 is the feed adsorbate concentration in the aqueous phase, q_0 is the adsorbate concentration in the solid phase in equilibrium with c_0; c and q are the adsorbate concentrations in the aqueous and solid phases, respectively [11].

In the linear driving force model, the uptake rate of adsorbate by a pellet is postulated as linearly proportional to a driving force. The driving force is defined as the difference between the surface concentration and the average adsorbed-phase concentration. In fixed bed adsorption, two-phase exchange models describing mass transfer rate can be established with linear driving force model based on concentration difference [12,13]. In the models, the mass transfer rate is expressed by using the overall mass transfer coefficient based on the fluid phase concentration difference as the driving force. Similarly, the mass transfer rate can also be expressed based on the solid phase concentration difference as the driving force. The former and latter models above are considered valid, at fluid-to-particle mass transfer and at intra-particle diffusion, respectively. In addition, adsorption equilibrium is considered to hold at the particle surface as $q_s = q_s(c_s)$ where q_s and c_s are the adsorbate concentrations in the solid and aqueous phases at the particle surface, respectively. The basic equations for mass transfer rate are as follows:

$$\rho_b dq/dt = k_f(c - c_s) = k_s(q_s - q) \tag{11}$$

where k_f is the fluid-to-particle mass transfer coefficient and k_s is the particle phase mass transfer coefficient. The particle phase mass transfer coefficient is related to the intra-particle diffusion parameters [14] by

$$k_s = \rho_b 15\phi_s D_s / r^2 \tag{12}$$

or

$$k_s = \frac{15\phi_s D_p / r^2}{q_0/c_0} \tag{13}$$

where ϕ_s is the correlation parameter, D_p is the pore diffusion coefficient ($cm^2\ s^{-1}$), D_s is the surface diffusion coefficient ($cm^2\ s^{-1}$) and r is the particle radius (cm). Eq. (12) is used when surface diffusion kinetics are controlling whilst Eq. (13) is used for dominant pore diffusion kinetics.

Using the constant pattern condition given in Eq. (10), Eq. (11) can be transformed into dimensionless form as

$$\frac{1}{1+\zeta}\frac{dy}{d\theta} = x - x_s = (1/\zeta)(y_s - y) \tag{14}$$

where

$$\zeta = \left(\frac{k_f}{k_s}\right)\left(\frac{c_0}{q_0}\right) \tag{15}$$

$$\theta = \frac{t - \varepsilon_b z/u}{1/k_f + 1/k_s(q_0/c_0)} \tag{16}$$

The other terms are $x = c/c_0$, $x_s = c_s/c_0$ where c_s is the aqueous solution concentration at the particle surface, $y = q/q_0$, and $y_s = q_s/q_0$ where q_s is the solid phase concentration at the particle surface.

The Langmuir isotherm equation will be used to relate the mechanics of adsorption of phenol onto the activated carbons for the fixed bed process. From the original expression of the Langmuir isotherm in Eq. (1), it can be rewritten as

$$y_e = \frac{x_e}{R + (1-R)x_e} \tag{17}$$

where $y_e (= q_e/q_0)$ and $x_e (= c_e/c_0)$ are the dimensionless concentrations at equilibrium. R is defined as a "constant separation factor" or "equilibrium parameter"

$$R = \frac{1}{1 + b_L c_0} \tag{18}$$

R represents the equilibrium characteristics of different systems as the mean concentration at any given cross-section in a fixed bed is given by x and y.

Using Eq. (17), Eq. (14) can be solved and the solution [14] is given as

$$\frac{K_s}{\rho_b}(t - t_0) = \frac{1}{1+\zeta}\left[\frac{1}{1-R}\ln x_s - \frac{R}{1-R}\ln(1-x_s) - \ln\{R + (1-R)x_s\} - \frac{R}{1-R}\ln R + 1\right] + \frac{\zeta}{1+\zeta}\left\{\frac{R}{1-R}\ln x_s - \frac{R}{1-R}\ln(1-x_s) - 1\right\} \tag{19}$$

where

$$\frac{1}{K_S} = \frac{q_0/c_0}{k_f} + \frac{1}{k_s} \tag{20}$$

and

$$t_0 = (z/u)[\varepsilon_b + \rho_b q_0/c_0] \tag{21}$$

The expression in Eq. (19) is based on x_s. Knowing x_s, x is obtained as follows:

$$x = [(\zeta R + 1)x_s + \zeta(1-R)x_s]/(\zeta + 1)[R + (1-R)x_s] \tag{22}$$

In the case of external mass transfer controlling the rate of adsorption or intra-particle diffusion being the sole rate-determining step, the above solution can be reduced to simpler forms in Eq. (23) for the LDFC model and Eq. (24) for the LDFQ model:

$$\frac{k_f}{\rho_b q_0/c_0}(t - t_0) = 1 - \frac{R\ln(1-x) - \ln x}{1-R} \tag{23}$$

$$\frac{k_s}{\rho_b}(t - t_0) = \frac{R}{1-R}\ln x - \frac{1}{1-R}\ln(1-x) - 1 \tag{24}$$

where t is the contact time.

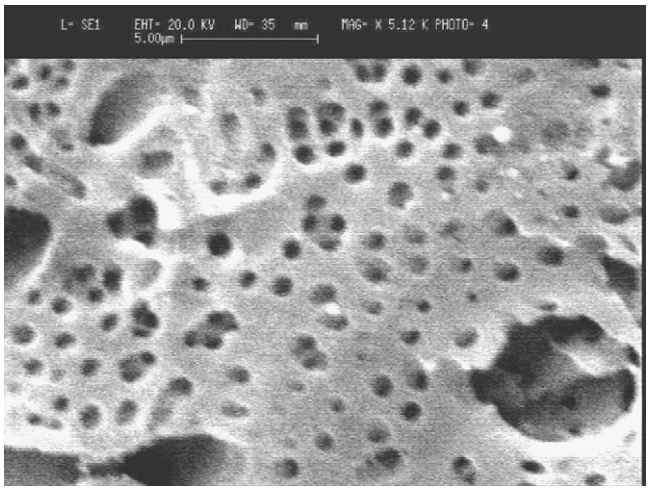

Fig. 1. Scanning electron micrograph of the activated carbon (5120×).

3. Experiment

3.1. Activated carbon preparation

The raw oil–palm shells were crushed and sieved to a size range of 2–2.8 mm. After drying at 110 °C in an electric oven for 24 h, the shells were placed in a vertical stainless steel reactor which was put in a tube furnace. The shells were heated under vacuum from room temperature to 400 °C at a heating rate of 10 °C/min. The sample was held at the final temperature for 2 h during pyrolysis. Subsequently, the resulting chars were removed and placed into another reactor for activation. In the physical activation process, the chars were heated under nitrogen atmosphere from room temperature to 900 °C at a heating rate of 10 °C/min. Having reached the final temperature of 900 °C, steam from an electric steam generator was introduced. The hold time during steam activation was 1 h. The resulting activated carbons were characterized using an accelerated surface area and porosimetry system (ASAP 2010, Micromeritics) under N_2 adsorption at −196 °C. Using the Brunauer–Emmett–Teller (BET) equation, data from the isotherms were used to determine the BET surface area [15]. The *t*-plot method was used to calculate the micropore volume [16]. The total pore volume was estimated to be the liquid volume of adsorbate (N_2) at a relative pressure of 0.985. The difference between the total pore volume and the micropore volume is the non-micropore volume. The pore size distribution of the activated carbon was obtained from the nitrogen adsorption isotherm using the density functional theory [16].

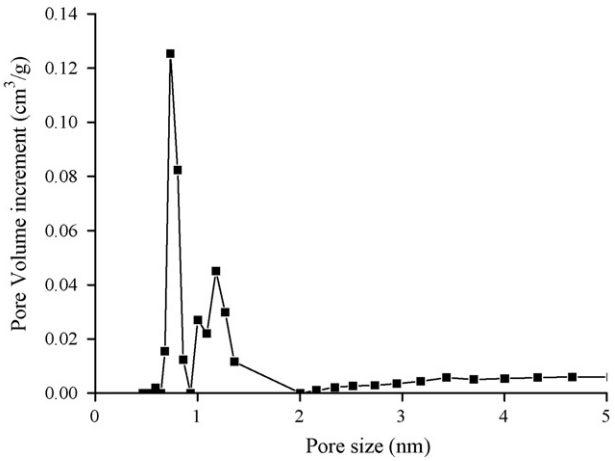

Fig. 2. Pore size distribution of the activated carbon.

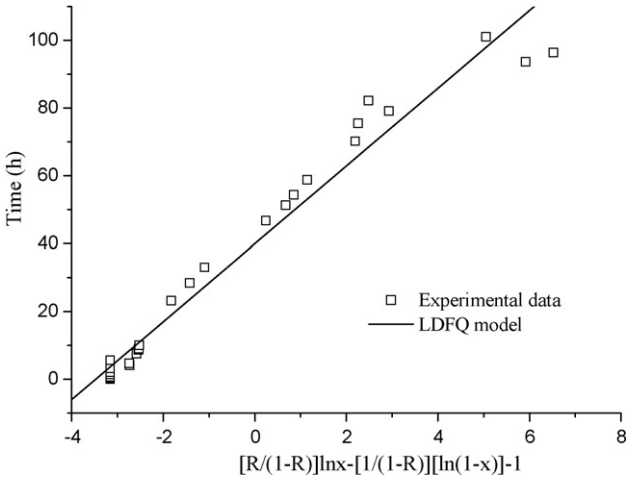

Fig. 3. Validity of the LDFQ model based on the Langmuir isotherm model.

Table 1
Physical characteristics of the activated carbon prepared from oil–palm shell.

BET surface area ($m^2\ g^{-1}$)	1183
Pore volume ($cm^3\ g^{-1}$)	0.69
Non-micropore surface area ($m^2\ g^{-1}$)	354
Non-micropore volume ($cm^3\ g^{-1}$)	0.38
Average pore size (nm)	2.33

Table 2
Experimental conditions of the fixed bed tests.

Flow rate	1 ml/min
Influent concentration	204 mg/l
Bed height	8.5 cm
Bed diameter	1.1 cm
Temperature	30 °C
Bed void fraction ε_b	0.4347
Bed density	0.48 g/cm^3

3.2. Dynamic experiment

Fixed bed adsorption was carried out in a glass column with an inside diameter of 1.1 cm and a length of 30 cm. The feed phenol solution was pumped through the column by a peristaltic pump

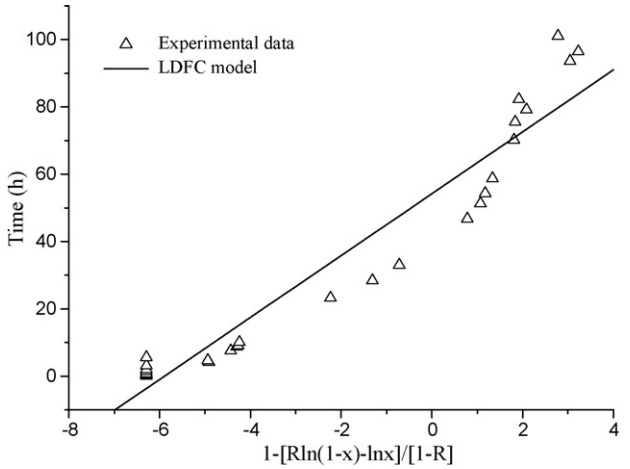

Fig. 4. Validity of the LDFC model based on the Langmuir isotherm model.

Table 3
Experimental conditions and correlation results of LDF models.

	LDFC model	LDFQ model
Correlation coefficient	0.97	0.98
t_0 (min)	3251.50	2393.90
Slope	551.88	689.33

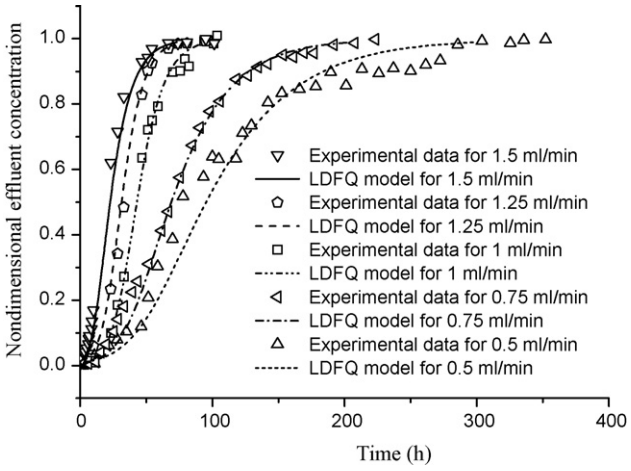

Fig. 5. Effect of flow rate on the breakthrough curve.

(Masterflux). The inlet to the pump was also connected to a de-ionized water supply through a three-way valve. Oil–palm-shell activated carbons with a known weight were packed into the column. The bed density and the void fraction were then determined. The activated carbons were flushed with de-ionized water for 12 h to remove any fine particles. The phenol solution was fed to the column in an upward flow direction at a desired flow rate by the peristaltic pump until breakthrough occurred. Samples for the determination of phenol concentration were taken from the effluent intermittently. The phenol concentration in the samples was determined by the gas chromatograph-mass spectrometer (6890N GC-5973 MSD system, Agilent).

4. Results and discussion

4.1. Activated carbon characterization

Fig. 1 shows the surface pore structure of the oil–palm-shell activated carbon used in the adsorption equilibrium and kinetic tests. The pores are generally homogeneous and distributed uniformly over the carbon surface. Fig. 2 shows the pore size distribution of the activated carbon using the density functional theory as described in Section 3.1; it consists of a microporous and mesoporous pore structure which is suitable for aqueous phase adsorption. Table 1 shows the physical characteristics of the activated carbon used in the adsorption studies. The high BET surface area of 1183 m^2/g renders the activated carbon to be a suitable adsorbent and its high non-micropore volume content of 55% of the total pore volume makes it a good adsorbent for aqueous phase applications.

4.2. Dynamic experiments

The axial dispersion Peclet number for the fixed bed was determined to evaluate the longitudinal dispersion. Axial dispersion coefficient accounts for the axial diffusion mechanism. The correlation presented by Chung and Wen [17] was used to determine the axial dispersion coefficient for liquids in fixed beds. The Peclet number was calculated using the correlation [18], $Pe = H/d_p\varepsilon_b(0.2 + 0.011Re_p^{0.48})$, where Re_p is the particle Reynolds number, $Re_p = u\varepsilon_b d_p\rho_f/\mu$, H is the column height, d_p is the particle diameter, ρ_f is the fluid density, and μ is the fluid dynamic viscosity. The operating conditions for a fixed bed run were a temperature of 30 °C, a feed flow rate of 1 ml/min, and a bed height of 85 mm. At these conditions, the Pe number of the bed was found to be 25.74. This value is considered large enough for ignoring the axial dispersion in the adsorption process. In addition, low flow rates were used in the tests to ensure that near local equilibrium conditions existed in the fixed bed.

4.3. Breakthrough dynamics

For the LDFC model, Eq. (23) can be re-arranged as follows:

$$t = t_0 + \frac{\rho_b q_0/c_0}{k_f}\left(1 - \frac{R\ln(1-x) - \ln x}{1-R}\right) \quad (25)$$

For the LDFQ model, Eq. (24) can be re-arranged as follows:

$$t = t_0 + \rho_b/k_s\left(\frac{R}{1-R}\ln x - \frac{1}{1-R}\ln(1-x) - 1\right) \quad (26)$$

Using the experimental adsorption data for the fixed bed, both the LDFQ and LDFC models are plotted in Figs. 3 and 4, respectively. The LDFQ model gives a better linear correlation with the experimental results than the LDFC model. The value of t_0 and the respective mass transfer coefficient k_s can be determined from the intercept and the slope of the line, respectively, as given in Eq. (26). The experimental conditions for the fixed bed tests and the correlation results are

Table 4
Adsorption parameters in the LDFQ model by non-linear regression of experimental data for different flow rates.

Flow rate (ml/min)	Influent concentration (mg/l)	Bed height (cm)	Adsorbent weight (g)	Mass transfer coefficient ($g\,cm^{-3}\,s^{-1}$)	Characteristic time, t_0 (h)	Equilibrium parameter R
0.50	203	8.80	2.92	$1.75e^{-4}$	112.80	0.32
0.75	203	8.20	2.90	$2.98e^{-4}$	75.70	0.32
1.00	204	8.50	2.93	$5.44e^{-4}$	44.40	0.36
1.25	201	8.50	2.91	$7.21e^{-4}$	32.10	0.37
1.50	206	8.40	2.91	$7.29e^{-4}$	25.20	0.31

Table 5
Adsorption parameters in the LDFQ model by non-linear regression of experimental data for different influent concentrations.

Influent concentration (mg/l)	Flow rate (ml/min)	Bed height (cm)	Adsorbent weight (g)	Mass transfer coefficient ($g\,cm^{-3}\,s^{-1}$)	Characteristics time, t_0 (h)	Equilibrium parameter R
395	1.00	8.60	2.93	$6.46e^{-4}$	28.60	0.31
204	1.00	8.50	2.93	$5.44e^{-4}$	44.40	0.36
115	1.00	8.20	2.92	$4.87e^{-4}$	54.00	0.37
54	1.00	8.50	2.91	$4.69e^{-4}$	60.00	0.38

Table 6
Adsorption parameters in the LDFQ model by non-linear regression of experimental data for different bed heights.

Bed height (cm)	Influent concentration (mg/l)	Flow rate (ml/min)	Adsorbent weight (g)	Mass transfer coefficient ($g\,cm^{-3}\,s^{-1}$)	Characteristics time, t_0 (h)	Equilibrium parameter R
5.00	191	1.00	2.51	$9.51e^{-4}$	23.30	0.36
8.50	204	1.00	2.93	$5.44e^{-4}$	44.40	0.36
13.00	209	1.00	3.52	$3.42e^{-4}$	58.00	0.36
17.00	216	1.00	4.09	$2.53e^{-4}$	71.60	0.37

given in Tables 2 and 3, respectively. Based on the results given in Figs. 3 and 4, as well as the correlation coefficient in Table 3, the LDFQ model was used to determine the breakthrough curves for the fixed bed.

4.4. Effects of fixed bed conditions on the breakthrough curves

The influences of the operation conditions, namely, the flow rate, the influent concentration and the fixed bed height, on the breakthrough curves were studied.

The effect of flow rate on the breakthrough curves is shown in Fig. 5. Five values of flow rate were investigated. The experimental values of the non-dimensional effluent concentration versus the time were plotted. Using the LDFQ model in Eq. (26), the theoretical breakthrough curves (x versus t) were also plotted in Fig. 5. The operating conditions of the tests and the adsorption parameters in the LDFQ model are given in Table 4.

In Fig. 5, the agreement between the experimental results and the LDFQ model is good. For a low flow rate, the breakthrough time is longer than that of a higher flow rate because it takes a longer time to reach its effective bed load if the other operating conditions are constant. Therefore, as the flow rate increases, the breakthrough curve becomes steeper because of the shorter time required to attain its effective bed load. In other words, increasing flow rate decreases the effective bed load or the effective adsorption capacity of the column of activated carbons. In Table 4, for increasing flow rate, i.e., increasing superficial velocity, the characteristic time decreases. This is to be expected because the effective bed load reduces with increasing flow rate and hence requires a shorter time for breakthrough of bed. Conversely, the mass transfer coefficient must increase for increasing flow rate as the column of activated carbons must adsorb its effective mass of adsorbate in a shorter time. This is reflected in Table 4 such that increasing flow rate increases the mass transfer coefficient.

The effect of influent concentration on the breakthrough curves is shown in Fig. 6 for four phenol feed concentrations of 54, 115, 204 and 395 mg/l. The operating conditions and the adsorption parameters in the LDFQ model are similarly given in Table 5. For a fixed temperature, changing the influent concentration will affect the breakthrough curve characteristics in two ways. First, increasing the influent concentration will reduce the time required to reach its effective bed load. Hence, the breakthrough curve becomes steeper as the influent concentration increases as shown in Fig. 6. Secondly, increasing the influent concentration will increase the adsorption rate of the activated carbons due to a higher concentration gradient and may increase the breakthrough time. However, from the breakthrough curves presented in Fig. 6, the first effect is more predominant and therefore the breakthrough time decreases for increasing influent concentration. The above trends can also be seen in Table 5. Decreasing influent concentration decreases the mass transfer coefficient but increases the characteristic time.

The effect of bed height on the breakthrough curves is shown in Fig. 7 for four bed heights of 5, 8.5, 13 and 17 cm. The operating conditions and the adsorption parameters in the LDFQ model are given in Table 6. In Fig. 7, increasing bed height increases the breakthrough time as expected. The mass transfer zone in a fixed bed travels from the entrance of the bed and progresses towards the exit. Hence, for the same influent phenol concentration and fixed bed conditions, an increase in the bed height results in a longer distance for the mass transfer zone to reach the exit and therefore an increase in the breakthrough time. This is correspondingly reflected in Table 6 in which the characteristic time increases with increasing bed height. Also, in the same table, the mass transfer coefficient increases as the bed height decreases. This implies that the adsorption or loading distribution along the bed height is the highest at the front face and gradually decreases towards the bed exit. In a random packing of activated carbons in a bed column, a carbon particle can be directly obstructed by another carbon particle in front of it, thereby reducing the exposure of the adsorbate molecules to the adsorbent and other adverse fluid flow effects. Hence, these adverse conditions increase with increasing bed height and reduce the mass transfer coefficient. In other words, the effective bed load per unit length decreases with increasing bed height.

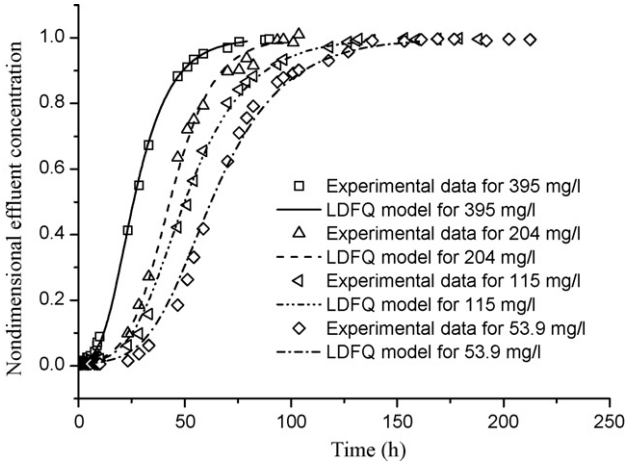

Fig. 6. Effect of influent concentration on the breakthrough curve.

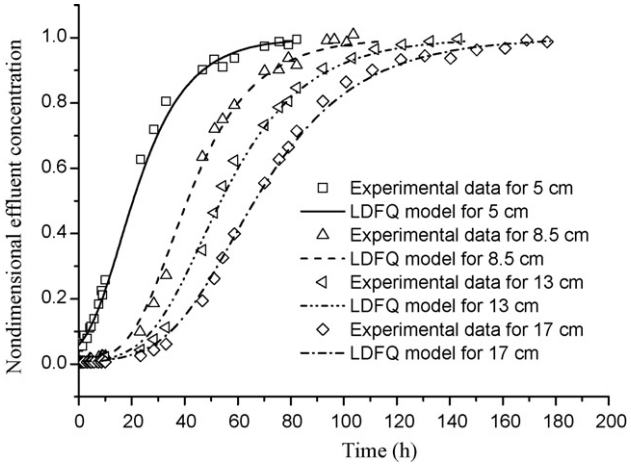

Fig. 7. Effect of bed height on the breakthrough curve.

5. Conclusions

In this work, activated carbons were prepared from oil–palm shells for removing phenol by aqueous phase adsorption. Series of column tests had been carried out for the adsorption of phenol by the activated carbons. Effects of operation conditions on the breakthrough curves were investigated.

Increasing flow rate in fixed bed adsorption resulted in steeper breakthrough curves, with shorter breakthrough times. For increasing phenol feed concentration, steeper breakthrough curve was obtained and breakthrough was reached earlier. With a smaller bed height, the ratio of the effluent to the influent adsorbate concentration reached unity more rapidly than that for a higher bed height.

Langmuir isotherm equation was used to model the adsorption equilibrium. The fixed bed results indicated that the phenol adsorption process by activated carbons could be described by the Langmuir isotherm equation. The comparison between the linear driving force models and the phenol adsorption results indicated that the intra-particle diffusion was the controlling step in the adsorption process. Therefore, the linear driving force model based on particle phase concentration difference was used to correlate the experimental results. With this LDFQ model, mass transfer coefficient, characteristic time and equilibrium parameter were obtained and the agreement between the model and the experimental results for the breakthrough curves was good.

References

[1] Toxicological profile for chlorophenols, Agency for Toxic Substances and Disease Registry, US Department of Health and Human Services, July 1999.
[2] C.S. Hottenstein, S.W. Jourdan, M.C. Hayes, F.M. Rubio, D.P. Herzog, T.S. Lawruk, Determination of pentachlorophenol in water and soil by a magnetic particle-based enzyme immunoassay, Environ. Sci. Technol. 29 (11) (1995) 2754–2758.
[3] J.M. Chern, Y.W. Chien, Adsorption of nitrophenol onto activated carbon: isotherms and breakthrough curves, Water Res. 36 (3) (2002) 647–655.
[4] B.C. Pan, F.W. Meng, X.Q. Chen, B.J. Pan, X.T. Li, W.M. Zhang, X. Zhang, J.L. Chen, Q.X. Zhang, Y. Sun, Application of an effective method in predicting breakthrough curves of fixed-bed adsorption onto resin adsorbent, J. Hazard. Mater. 124 (1–3) (2005) 74–80.
[5] Z. Husain, Z.A. Zainal, M.Z. Abdullah, Analysis of biomass-residue-based cogeneration system in palm oil mills, Biomass Bioenergy 24 (2) (2003) 117–124.
[6] J. Guo, A.C. Lua, Characterization of adsorbent prepared from oil–palm shell by CO_2 activation for removal of gaseous pollutants, Mater. Lett. 55 (5) (2002) 334–339.
[7] Q. Jia, A.C. Lua, Effects of pyrolysis conditions on the physical characteristics of oil–palm-shell activated carbons used in aqueous phase phenol adsorption, J. Anal. Appl. Pyrol. 83 (2) (2008) 175–179.
[8] Q. Jia, A.C. Lua, Concentration-dependent branched pore kinetic model for aqueous phase adsorption, Chem. Eng. J. 136 (2–3) (2008) 227–235.
[9] J.L. Sotelo, M.A. Uguina, J.A. Delgado, L.I. Celemin, Adsorption of methyl ethyl ketone and trichloroethene from aqueous solutions onto activated carbon fixed-bed adsorbers, Sep. Purif. Technol. 37 (2) (2004) 149–160.
[10] G.S. Bohart, E.Q. Adams, Some aspects of the behavior of charcoal with respect to chlorine, J. Am. Chem. Soc. 42 (3) (1920) 523–544.
[11] J.M. Chern, Y.W. Chien, Adsorption isotherms of benzoic acid onto activated carbon and breakthrough curves in fixed-bed columns, Ind. Eng. Chem. Res. 40 (17) (2001) 3775–3780.
[12] M. Otero, M. Zabkova, A.E. Rodrigues, Adsorptive purification of phenol wastewaters: experimental basis and operation of a parametric pumping unit, Chem. Eng. J. 110 (1–3) (2005) 101–111.
[13] F.C. Gazola, M.R. Pereira, M.A.S.D. Barros, E.A. Silva, P.A. Arroyo, Removal of Cr^{3+} in fixed bed using zeolite NaY, Chem. Eng. J. 117 (3) (2006) 253–261.
[14] M. Suzuki, Adsorption Engineering, Elsevier, Amsterdam, 1990.
[15] S.J. Gregg, K.S.W. Sing, Adsorption, Surface Area, and Porosity, Academic Press, London, 1982.
[16] P.A. Webb, C. Orr, Micromeritics Instrument Corporation. Analytical Methods in Fine Particle Technology, Micromeritics Instrument Corporation, Norcross, GA, 1997.
[17] S.F. Chung, C.Y. Wen, Longitudinal dispersion of liquid flowing through fixed and fluidized beds, AIChE J. 14 (6) (1968) 857–866.
[18] A.E. Rodrigues, J.M. Loureiro, M.R. de la Vega, Fixed-bed irreversible adsorption with pore diffusion and axial dispersion, AIChE J. 51 (12) (2005) 3286–3291.